Journal of Power Sources 195 (2010) 1393–1400

Contents lists available at ScienceDirect

Journal of Power Sources

journal homepage: www.elsevier.com/locate/jpowsour

Experimental study of a novel piezoelectric proton exchange membrane fuel cell with nozzle and diffuser

Hsiao-Kang Ma*, Shih-Han Huang, Jyun-Sheng Wang, Churng-Guang Hou, Chen-Chiang Yu, Bo-Ren Chen

Department of Mechanical Engineering, National Taiwan University, Taipei 10617, Taiwan, ROC

ARTICLE INFO

Article history:
Received 28 July 2009
Received in revised form
13 September 2009
Accepted 14 September 2009
Available online 20 September 2009

Keywords:
Piezoelectric
Fuel cell
Nozzle
Diffuser
Frequency
Air-breathing

ABSTRACT

The newly designed proton exchange membrane fuel cell with a piezoelectric actuation structure, called a PZT-PEMFC, can force air into an air-breathing PEMFC system. Previous studies indicated the PZT-PEMFC may solve the water-flooding problem and improve cell performance. In this experimental study, a PZT-PEMFC with nozzle and diffuser, PZT-PEMFC-ND, is built to verify the previous theoretical study. This innovative design may direct air flow into the cathode channel through the diffuser and prevent air backflow without valves. The performance test includes an analysis of PZT vibration frequencies, cell operation temperatures, gravity effect, and designs of the nozzle and diffuser. The optimal operating temperature for the PZT-PEMFC-ND is 323 K to avoid the risk of higher temperatures drying out the membrane electrode assembly (MEA). The optimal vibration frequency of the PZT-PEMFC-ND is 180 Hz, which may pump in enough air and solve the water-flooding problem in the cathode channel. This study also concludes that the innovative design of the PZT-PEMFC-ND, may reach the performance of an open cathode stack configuration, 0.18 W cm^{-2}, without an external air supply device.

1. Introduction

Previous studies [1–4] indicated each flow field design of the PEMFC may have different fuel cell performances. For the interdigitated flow field, the reactant gas can be delivered to the catalyst layer and increase the electrochemical reaction rate. However, the pin-type flow fields have a lower reactant pressure, uneven gas distribution, poor water removal, and poor cell performance. On the other hand, the parallel flow field with an incorporated baffle exhibits better performance because the baffle effect forces the reactant gas to pass through the diffusion layer. The single-serpentine flow field exhibits better performance than double- and triple-serpentine flow fields. Most studies have indicated the serpentine field may lead to better performance than other flow field designs. Therefore, the serpentine flow field is another important study topic. In addition, a new convection-enhanced serpentine flow field has been proposed to increase the mass transport rate and remove liquid water trapped in the porous media [5].

Air-breathing proton exchange membrane fuel cells (AB-PEMFCs) have attracted attention because they do not need an additional oxygen supply device. The chemical reactions in AB-PEMFCs mainly depend on natural convection, which is caused by temperature and oxygen concentration gradients [6]. In order to deliver sufficient oxygen into the cathode channel, an open-air cathode PEMFC stack with a fan as the oxygen supplier was proposed [7]. In addition, dehydrating phenomena slightly affected the performance of AB-PEMFCs [8]. Moreover, catalyst loading, relative humidity, temperature, hydrogen stoichiometry, gas-diffusion layer thickness, and cathode structure are important parameters in the performance of AB-PEMFCs [9,10]. The open-air direction is another important parameter in air-breathing PEMFCs. The upward open-air direction may have better performance than the downward free-convection mode [11].

During AB-PEMFC operation, liquid water is transported by electro-osmotic drag, back diffusion, and convection in the membrane. The electro-osmotic drag coefficient has been found to be a function of the water content of the membrane and temperature [12–15]. Water content is the ratio of water molecules to the number of charge ($SO_3^-H^+$) sites, which is an important parameter to determine the activity of water vapor between the membrane and electrode interface [16]. Generally, the electro-osmotic drag coefficient increases with increasing water content in the membrane. At high water content, the electro-osmotic drag coefficient increases with increasing temperature. Yi and Nguyen [17] showed that PEMFC performance was improved by anode humidification and positive differential pressure between the cathode and anode, which is also proved by the Nernst equation. Ge and Yi [18] pre-

* Corresponding author. Tel.: +886 2 23629976; fax: +886 2 23631755.
E-mail address: skma@ntu.edu.tw (H.-K. Ma).

0378-7753/$ – see front matter © 2009 Elsevier B.V. All rights reserved.
doi:10.1016/j.jpowsour.2009.09.033

Nomenclature

A	cross section area
A_{PZT}	piezoelectric area (m^2)
AR	aspect ratio
C	conductivity coefficient
D	channel opening width
f	frequency of PZT (Hz)
k	proportionality constant
L	channel path
P	pressure ($N\,m^{-2}$)
P_c	channel pressure
P_{in}	inlet pressure
P_{out}	outlet pressure
R	gas constant ($J\,mol^{-1}\,K^{-1}$)
Re	Reynolds number
t	time (s)
T	temperature (K)
V_c	cathode inlet velocity ($m\,s^{-1}$)
V_{PZT}	motion equation of the piezoelectric device ($m\,s^{-1}$)

Greek letters

ζ	loss coefficient
θ	diffuser angle
ρ	density ($kg\,m^{-3}$)
$\forall$	volume displacement (m^3)
$\forall_0$	amplitude volume (m^3)

dicted that the dry reactant gases would be successfully humidified internally and would maintain high performance when the PEMFC was operated in counter-flow mode. Thus, water transport and management is dependent upon the structure and properties of the cell components, reactant stream humidification, flow field layout, and structural and wetting properties of the gas-diffusion media and micro porous layer [19].

The micropump has been developed with several actuation methods, including piezoelectric (PZT), electromagnetic, shape memory alloy, electrostatic, and thermo-pneumatic devices. However, most of them have complex structures and low pumping performance. Micro-diaphragm pumps are classified based on the presence or absence of valves [20,21]. For fuel cell applications, a gas pump with a novel bimorph actuation structure can also feed air into the micro direct methanol fuel cell (DMFC) [22]. These results showed that the air-diaphragm pump worked at a flow rate of 85.3 ml min^{-1} in resonance with 3.18 mW, and at a low-power consumption of below 20 V. Previous studies [23–27] indicated that a novel design for proton exchange membrane fuel cells with a piezoelectric device, PZT-PEMFC, which is regarded as an actuator for pumping air onto the cathode channel, can offer better performance with higher current generation. The novel design of PZT-PEMFC is applied in the micro system with a low-power unit. Although an external air blower or fan may suck enough air into the cathode channel and increase current generation, they require higher power and larger space. Thus, the smaller PZT device has an advantage to replace the existed air blower or fan in a micro PEMFC system. Previous results also indicate that a PZT-PEMFC can compress more air into the catalyst layer and thus enhance electrochemical reactions, resulting in higher current output. At the same time, produced water vapor is pumped out from the cathode channel.

The objective of this study is to build a PZT-PEMFC with a nozzle and diffuser, a PZT-PEMFC-ND, and prove that this innovative design could solve the water-flooding problem and improve cell performance. The experimental parameters include PZT vibration

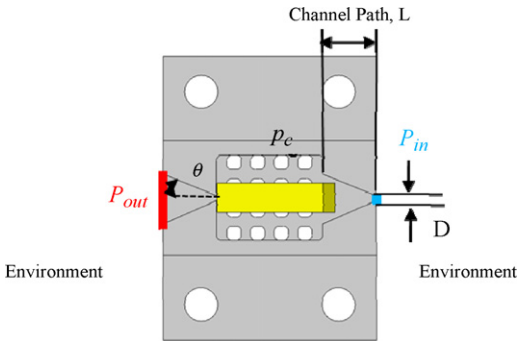

Fig. 1. The cathode channel design of a PZT-PEMFC.

frequency, cell operation temperature, gravity effect, current density, and design of nozzle and diffuser.

2. Design of the air-breathing PZT-PEMFC-ND

The PZT-PEMFC without valves may attract the air into the cathode channel; however, both the channel path (L) and the channel opening width (D) of the cathode channel affect the cell performance. If the channel path is too long, the pressure in the cathode channel will be dissipated by friction in the channel path, as shown in Fig. 1. The efficiency ratio of a micropump diffuser depends on its geometry and Reynolds number [28–30]. Ahmadian and Mehrabian [30] concluded the optimized diffuser angle, ODA, can be written as a function of actuation pressure, AP. If it is desired to set high actuation pressures, smaller diffuser angles should be utilized in order to approach the maximum possible rectification of the diffuser. Thus, the PZT-PEMFC-ND, which is shown in Fig. 2, is proposed to direct more the air flow into the cathode [31,32].

Fig. 3 shows that the pumping process has three steps: transition mode ($P_{out} > P_c > P_{in}$), supply mode ($P_{out} > P_{in} > P_c$), and pump mode ($P_c > P_{out} > P_{in}$) [33]. The inlet pressure, P_{in}, is always smaller than the outlet pressure, P_{out}, an assumption due to the nozzle/diffuser design. In supply mode, the diaphragm moves outward and increases the cathode channel volume, which causes the chamber pressure to be lower than the atmospheric pressure thus sucking air into the chamber. In pump mode, the diaphragm moves inward and causes the cathode channel volume to decrease. Because the pressure inside the cell is higher than atmospheric pressure, the air is pushed into the catalyst layer and the produced

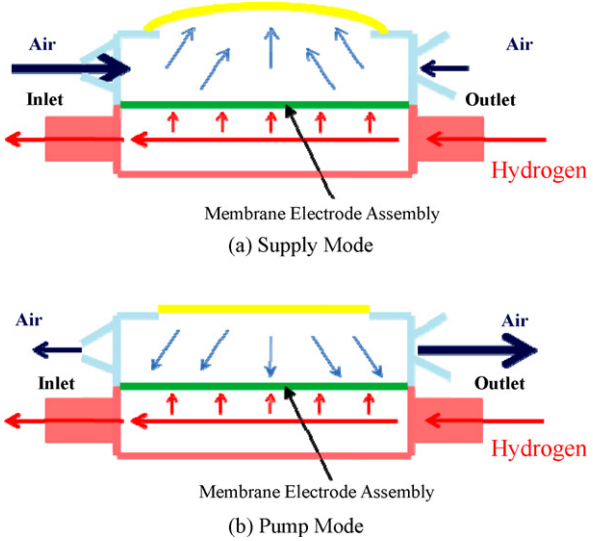

Fig. 2. The operation of the PZT-PEMFC.

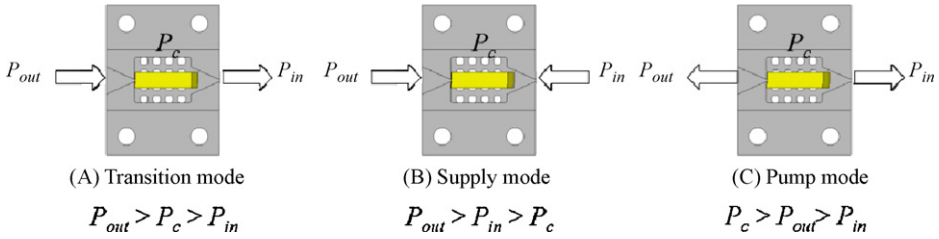

Fig. 3. The flow modes during pumping process.

water is pumped out of the cell. Between pump mode and supply mode there is a transition mode, which occurs when outlet pressure is higher than chamber pressure and inlet pressure, $P_{out} > P_c > P_{in}$.

The orientation of the nozzle/diffuser and the position of the PZT device are important parameters for the PZT-PEMFC due to its pumping efficiency and pressure distribution in the cathode channel. For this study, a one-sided actuator was chosen; therefore, the position of maximum PZT deformation was decided by the fixed side of PZT. Fig. 4 shows that there are three directions of the nozzle and diffuser: up, down, and horizontal.

The driving forces at the anode and cathode inlets are different in PZT-PEMFC-ND systems. The hydrogen is supplied from the hydrogen storage bottle, and hydrogen flow rate at the anode is controlled by a mass flow controller. In this study, the hydrogen mass flow rate is always a constant, 60 ml min^{-1}. On the other hand, the air flow at the cathode is driven by PZT vibrations.

For analyzing air flow rate of the PZT-PEMFC-ND system, the control volume of the system is chosen in the cathode channel (Fig. 5). The inlet velocity V is divided into the anode velocity V_a and cathode velocity V_c due to different supply methods. The equation of motion for the PZT device is a sine function, which is given by Eq. (1).

$$\vec{V}_{PZT} = \frac{d}{dt}\left[-0.0005 \times (\sin(2\pi ft))\right] \quad (1)$$

The inflow and outflow periods in the channel as induced by the sine/step function. The inlet velocity at the cathode, $\vec{V}_c$, is derived by the Reynolds Transport Theorem [23,24] as:

$$\vec{V}_c = \frac{1}{\rho A}\left[\frac{1}{R}\frac{\partial}{\partial t}\int_{C\forall}\frac{P}{T}d\forall + \rho\vec{V}_{PZT}A_{PZT}\right] \quad (2)$$

Thus, the flow rate can be written as:

$$Q_c = \frac{1}{R}\frac{\partial}{\partial t}\int_{C\forall}\frac{P}{T}d\forall + \rho\vec{V}_{PZT}A_{PZT} \quad (3)$$

The lumped system is a simple method for analyzing the valveless micropump, which is proposed by Ullmann [34]. This method neglected the spatial variation and focused on the time variation, which does not need complex CFD methods such as Navier-Stokes equations. The method was carried out for the three regions: pump mode, supply mode, and transition mode. This method also validated nozzle/diffuser design and compared it with the CFD method [33]. The results indicated that the agreements of these two methods are quite different in transition mode due to neglect of the inertial effect. Pan et al. [35] proved the inertial force could not be neglected, as compared with viscous loss. The cross section area of the cathode side in PZT-PEMFC-ND is shown in Fig. 1.

The pressure loss in the nozzle can be expressed in terms of the loss coefficient, ξ, from Eq. (4), which is an important parameter for

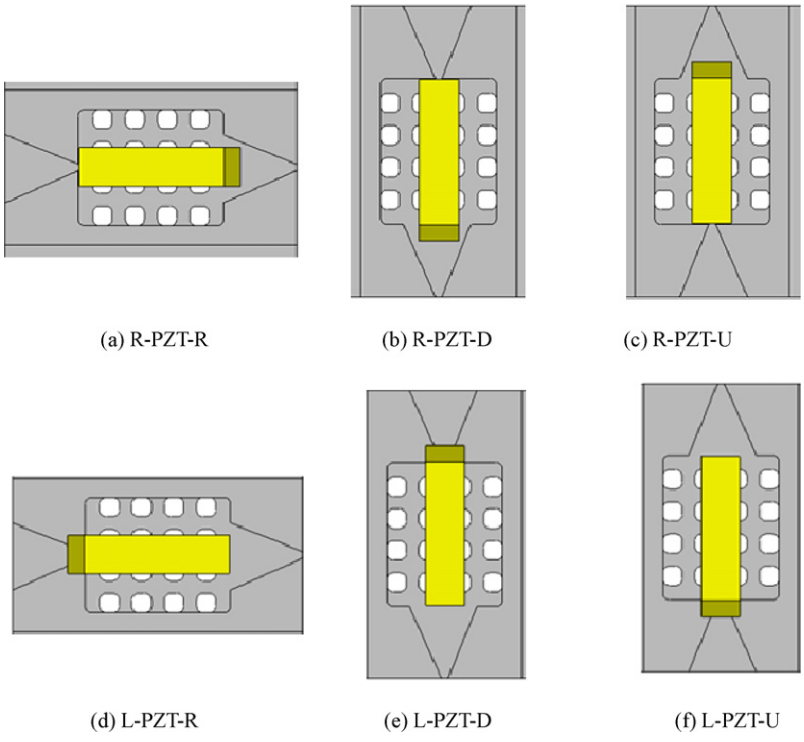

Fig. 4. The different directions of nozzle and direction and different PZT fix locations.

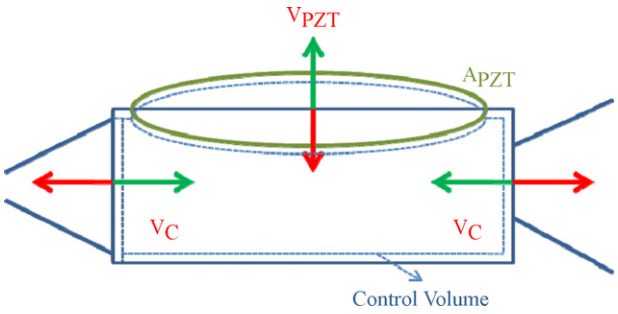

Fig. 5. The diagram of control volume in PZT-PEMFC.

nozzle and diffuser.

$$\Delta P = \frac{1}{2}\xi\rho\bar{V}^2 \tag{4}$$

where $\vec{V}$ is the mean velocity at the narrowest part of the nozzle/diffuser. In addition, the loss coefficients of nozzle/diffuser include three parts: inlet, exit, and nozzle/diffuser [36–41].

The diaphragm of the PZT-PEMFC-ND is the PDMS, which is assumed as a sinusoidal motion. With no pressure difference acting on the PDMS, the volumetric amplitude is $\forall_0$. On the other hand, the maximum volumetric displacement is $2\forall_0$. In addition, the PZT vibrates with time; thus, the volume displacement is also a function of time,

$$\forall = \forall_0 [1 - \cos(2\pi ft)] \tag{5}$$

$$\forall_0 = k(P_b - P_{atm}) \tag{6}$$

where P_b is the blocking pressure. The volume change can be written as Eq. (7):

$$\Delta\forall = \forall_0 \left[\frac{(P - P_{atm})}{(P_b - P_{atm})}\right] \tag{7}$$

The blocking pressure, P_b, is associated with stiffness value; therefore, the volume change rate can be written as Eq. (8):

$$\frac{d\forall}{dt} = 2\pi f\forall_0 \sin(2\pi ft) - \forall_0 \left[\frac{dP/dt}{(P_b - P_{atm})}\right] \tag{8}$$

The same theory can be applied to the air flow rate in the cathode channel of PZT-PEMFC-ND. Then, the inlet flow rate can be found as:

$$Q_{in,l} = C_n\sqrt{(P_{in} - P_c)} \quad \text{for the air flow from left to right, shown in Fig. 5} \tag{9}$$

$$Q_{in,r} = C_d\sqrt{(P_c - P_{in})} \quad \text{for the air flow from right to left,shown in Fig. 5} \tag{10}$$

where the conductivity coefficient can be separated into nozzle, C_n, and diffuser, C_d.

$$C_n = \frac{A}{\sqrt{(1/2)\xi_n\rho}} \tag{11}$$

$$C_d = \frac{A}{\sqrt{(1/2)\xi_d\rho}} \tag{12}$$

Although the net flow rate can be calculated from this method, the outflow rate is irrelevant to this study. The major reason is that the air in the cathode channel is reacted through the electrochemical reaction.

3. Experimental set-up

Fig. 6 shows the test platform for analyzing the PZT-PEMFC-ND performance. On the anode side, the hydrogen is humidified under a different temperature due to its different fuel and air composition. High pressure hydrogen from the hydrogen storage flows to the mass flow controller, then enters the humidifier. The humidifier is a water tank with a heater, which the reactant gas passes through at a specific temperature. Then, the hydrogen with water is delivered to the PZT-PEMFC-ND for the electrochemical reaction.

The equipment on the cathode side is more complex than on the anode side. First, the sine-wave signal of PZT vibrations is generated by a function generator. Next, the signal from the function generator goes to an amplifier to magnify the signal for a piezoelectric device. The piezoelectric device then vibrates when it receives the signal.

The PZT device of the PZT-PEMFC-ND is driven by a 150 V sine-wave signal generated by a function generator, which may supply air to the cathode side. The amplifier is required to magnify voltage to the designated dB. The vibration frequency of the PZT device is shifted from 0 Hz to 210 Hz; thus, the PZT device controls the air

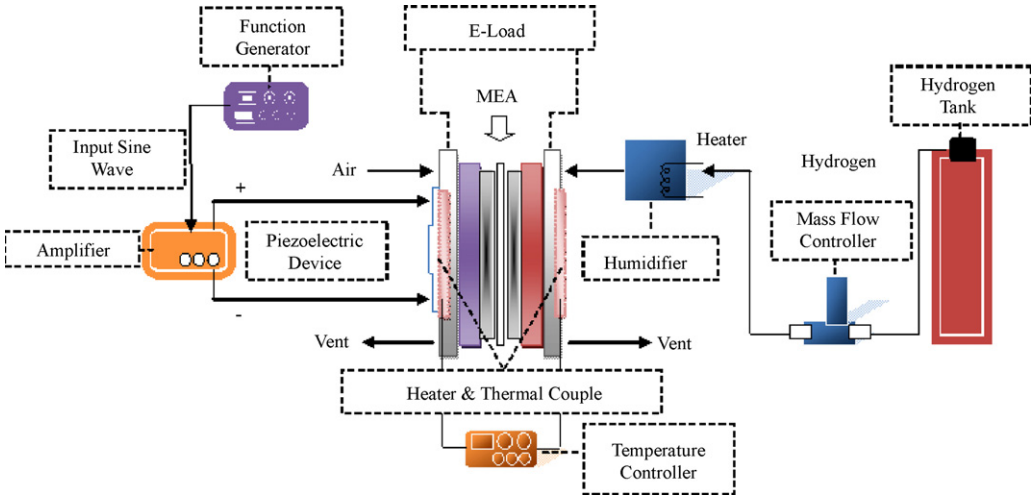

Fig. 6. Schematic of the PZT-PEMFC testing system.

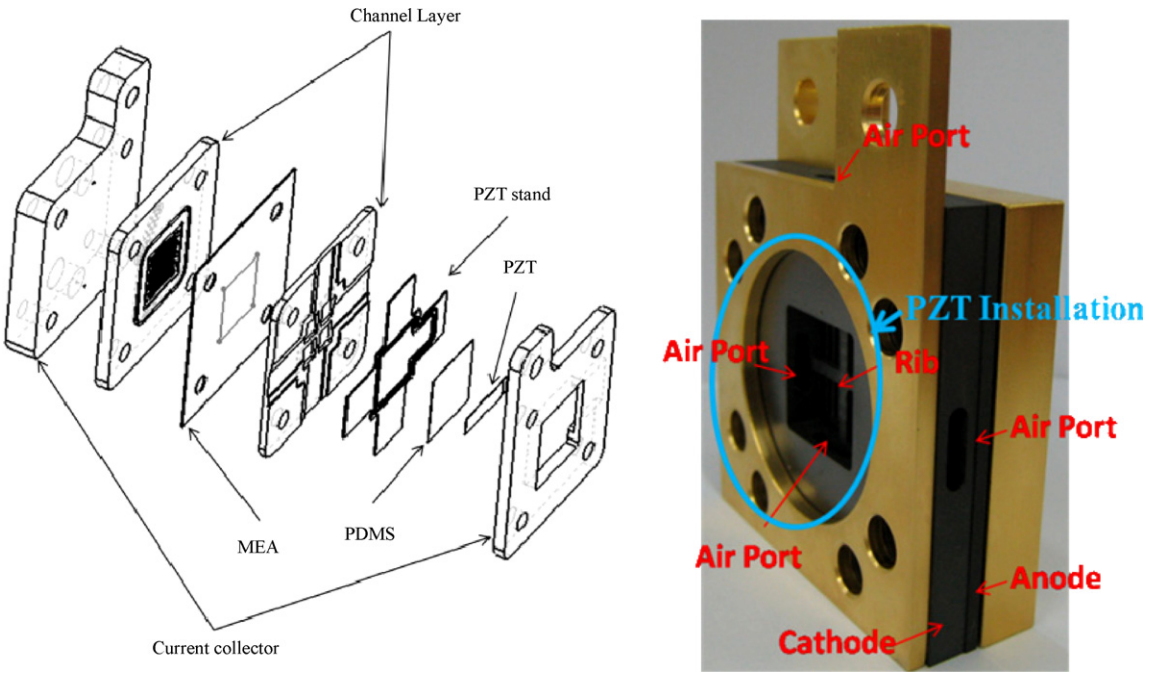

Fig. 7. An exploded drawing of PZT-PEMFC.

flow on the cathode side. In the anode side, the humidified hydrogen, under a temperature of 303 K to 343 K, flows into the anode channel. The hydrogen in the anode side is supplied by hydrogen storage and controlled by the mass flow controller at 60 ml min^{-1}. The DC electronic load can simulate the electronic loading of voltage and current. In this study, a constant voltage mode was chosen, and power output data was recorded for every 0.1 V from open circuit voltage to 0.2 V by using LabVIEW software.

The PZT-PEMFC-ND, which is shown in Fig. 7, is composed of two current collectors, two flow field plates, one membrane electrode

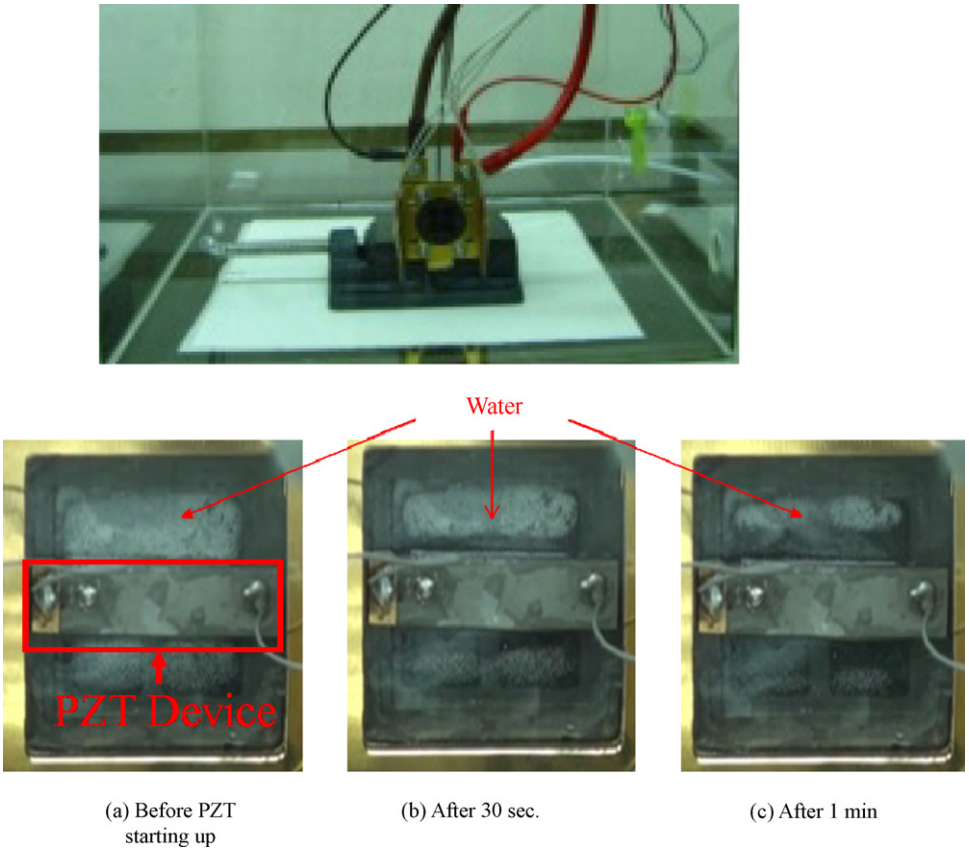

Fig. 8. Photos showing water removal within 1 min.

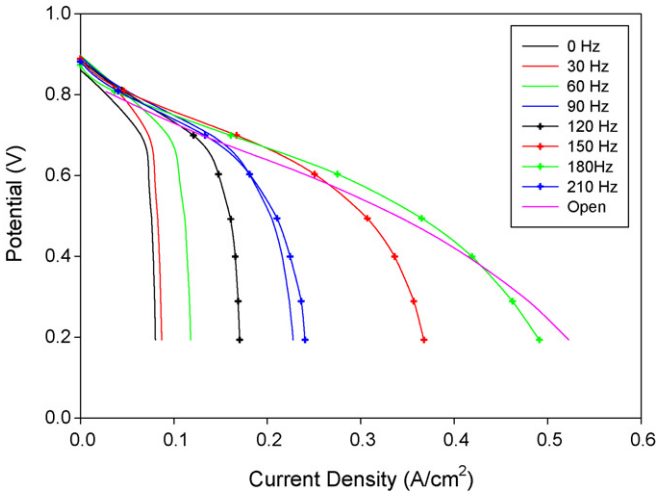

Fig. 9. The *I–V* curves under different PZT vibration frequencies at $T = 50\,^{\circ}C$.

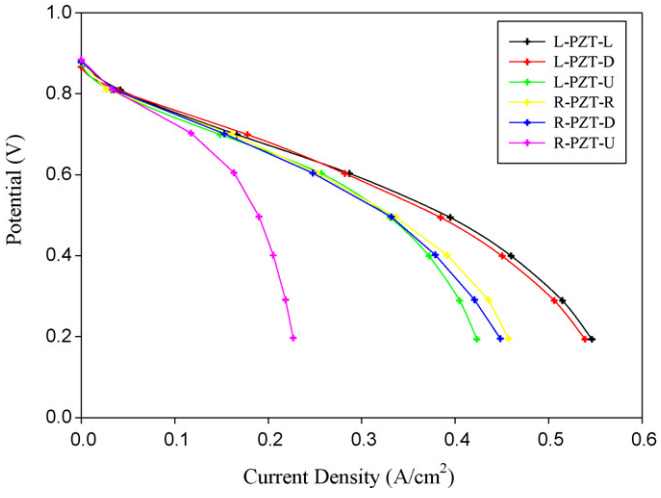

Fig. 11. The *I–V* curves under different gravity and vibration effects.

assembly (MEA), one PZT device, and a PZT stand. The reactive area of the MEA is 2 cm × 2 cm, the membrane is Nafion®212, and the ratio of open-air and reactive areas is 49% in the cathode. The PZT pump, which is made of PDMS, is attached to a gasket film to prevent gas leakage and to increase the volume change of the cathode channel.

4. Results and discussion

The experimental results indicated that the previous design of PZT-PEMFC may not reach the same performance as the open cathode case. Therefore, the nozzle and diffuser were applied between the environment and cathode channel, which may induce more air flow into the cathode channel, solve the water-flooding problem, and increase the cell performance. Fig. 8a shows the presence of accumulated water in the cathode channel, which cannot be removed from the cathode side. However, the amount of water is reduced in the cathode channel once the PZT starts to vibrate within 30 s (Fig. 8b). After 1 min, most of the water is pumped out from the cathode channel (Fig. 8c). These results show that PZT-PEMFC-ND solves the water-flooding problem in the cathode side, and proves that the theoretical study of the PZT-PEMFC can be carried out in an experimental study.

4.1. The effect of PZT-PEMFC-ND under different PZT vibration frequencies

A previous study [31] indicated that the PZT device, acted as the PZT pump in the cathode channel, providing insufficient air for an electrochemical reaction. Therefore, the nozzle and diffuser are used in the cathode side. The actuation force of the fluid motion depends on PZT material, chamber size, and PZT vibration frequency. While the designed PZT device is operated at a harmonic frequency, the cell performance can be improved by sucking more air into the chamber and pumping more water out. In this study the PZT harmonic frequencies are found near 90 Hz and 180 Hz. The *I–V* curves of $f = 0$ Hz and $f = 30$ Hz have almost the same poor cell performance because of low pumping efficiency due to less air being sucked into the cathode channel (Fig. 9). At PZT vibration frequencies of $f = 60$ Hz and $f = 90$ Hz, more air is sucked in and more water pumped out to prevent water-flooding in the cathode side; thus, cell performance improves. However, at $f = 120$ Hz, the *I–V* curve does not show continuous improvement due to the inharmonic resonance of the design. At the PZT vibration frequencies of $f = 150$ Hz and $f = 180$ Hz, cell performance greatly improves. The maximum current reaches 0.49 A cm^{-2} at $f = 180$ Hz, which is almost six times greater than the case without PZT vibration, $f = 0$ Hz. Considering the air stoichiometric ratio, the maximum current of PZT-PEMFC-ND is around 2 A; there-

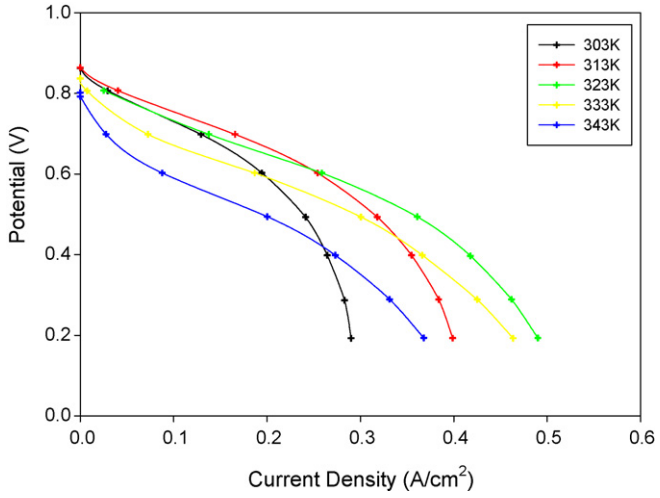

Fig. 10. The *I–V* curves under different operation temperatures at $f = 180$ Hz.

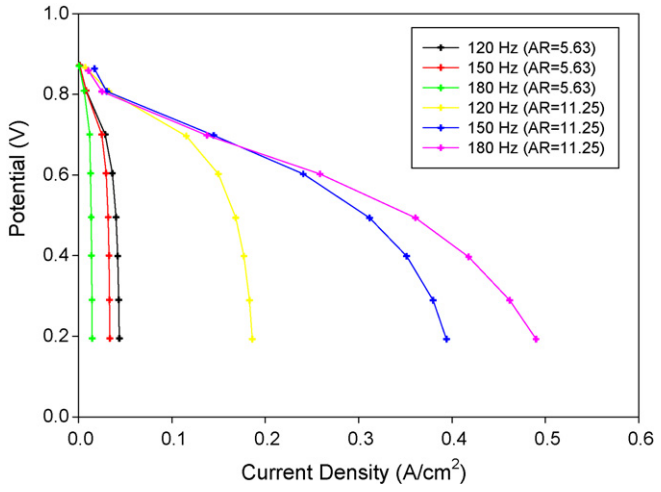

Fig. 12. *I–V* curves under different designs of nozzle and diffuser in PZT-PEMFC.

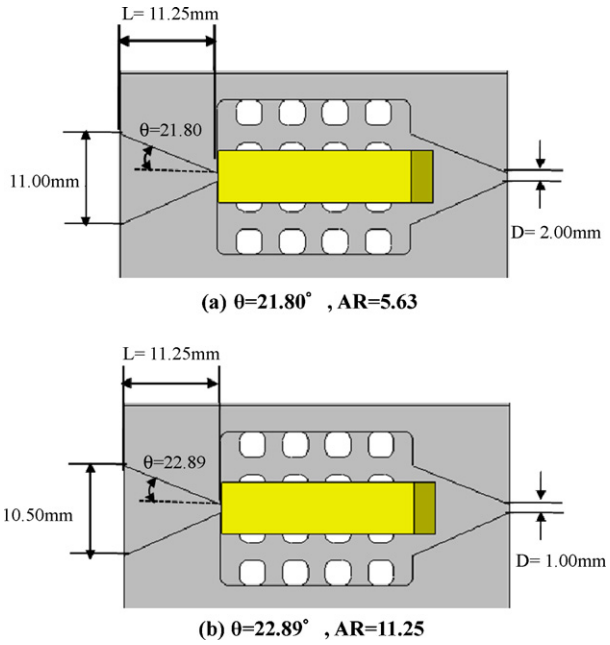

Fig. 13. Different designs of nozzle and diffuser in PZT-PEMFC.

fore, the air flow rate of the PZT-PEMFC-ND is 35 ml min^{-1} at least. Additionally, maximum power can reach 0.18 W cm^{-2} at f = 180 Hz, which is approximately four times greater than the case without PZT vibration, f = 0 Hz. This phenomenon proves that sufficient air intake is needed to overcome the concentration losses under certain PZT vibration frequencies. However, when a frequency of 210 Hz is applied, the efficiency of the cell immediately drops due to the inharmonic vibration of the PZT device. These results show that the PZT-PEMFC-ND does work, thus solving the water-flooding problem in the cathode and improving cell performance to equal the performance of the open cathode design.

4.2. The effect of operation temperature

Previous studies [42,43] showed that an appropriate increase in cell temperature is an important parameter to ensure high cell performance. Fig. 10 shows *I–V* curves at different temperatures under the PZT vibration frequency of 180 Hz. As the temperature increases from 303 K to 323 K, the average current density and cell performance also increases. This is because a high cell temperature improves the chemical reaction rate. In addition, the current density and cell performance decrease as temperature increases from 323 K to 343 K. This is because the membrane dries out under high temperatures. On the contrary, serious water-flooding can be seen in open cathodes at an operation temperature of 303 K. This flooding problem can be solved by adding a PZT device on the cathode channel, which is shown in Fig. 8.

4.3. The gravity and vibration effect for PZT-PEMFC-ND

The gravity effect may affect the water removal ability and air intake of a PZT-PEMFC-ND with a nozzle/diffuser design. Fig. 11 shows that different nozzle/diffuser orientations result in different cell performances. The cases of L-PZT-R and L-PZT-D (Fig. 4) have similar performances; however, the performance of the L-PZT-U decreases in the region of concentration losses. The reason is that the produced liquid water blocks the exit of the nozzle/diffuser due to gravity, and cannot be removed from the cathode channel. Thus, fresh air cannot be sucked from the nozzle into the cathode side. Additionally, the location of the maximum deflection of PZT vibration in the nozzle/diffuser also affects cell performance. Results indicate that the performances of the cases of the R-PZT are lower than the cases of the L-PZT. The main reason is that the maximum deflection may induce a higher pressure difference near the outlet (nozzle); however, the maximum pressure difference must be induced near the inlet (diffuser) to attract the most air in supply mode under the cases of R-PZT. Therefore, the gravity and the orientation of maximum deflection of PZT vibration may affect air intake, water removal rate, and cell performance. The cases of L-PZT-R and L-PZT-D are the better designs in this study.

4.4. Influence of nozzle and diffuser

The pump performance of PZT-PEMFC-ND is a function of geometry parameters, aspect ratio (AR) and diffuser angle (θ). Fig. 12 indicates that the geometries of the nozzle/diffuser in the PZT-PEMFC-ND influence the *I–V* curve significantly. In order to have optimal pump efficiency, a larger value for the diffuser angle (θ) should be chosen when the Reynolds number is decreasing. In this study, the diffuser angle is around 21–23° due to the lower average Reynolds number. For a lower AR of 5.63, as shown in Fig. 13a, the *I–V* curves drop in the regions of ohmic and concentration losses due to the low pump efficiency. On the other hand, the higher AR of 11.25 may induce a higher air flow rate into the cathode channel, and thereby increase the cell performance in the *I–V* curve. Fig. 14 indicates that the pressure of the higher AR design is twice that of the lower AR design. If the pressure between channel and atmosphere is not strong enough, sufficient air cannot be attracted into the cathode channel. Therefore, the AR of the nozzle and diffuser is an important parameter for PZT-PEMFC-ND performance. The optimal AR is 11.25 under θ = 22.89° in this study.

4.5. Required power of PZT-PEMFC-ND

The PZT-PEMFC-ND, which needs 50–150 V and a low current a 0.1–0.01 A, is suitable to be installed as a stack or as a part of stack for removing the water. The stack can be installed with a DC–AC

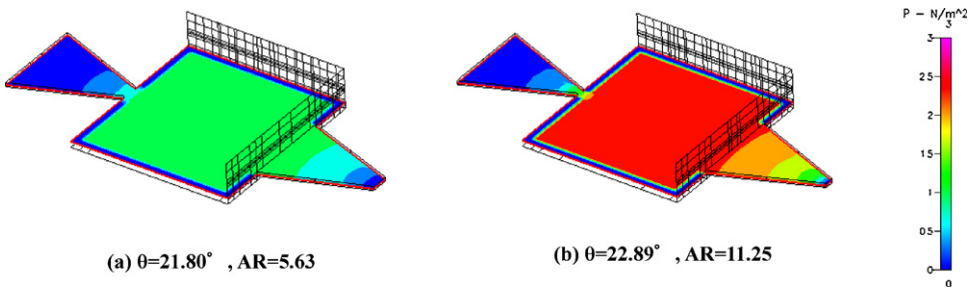

Fig. 14. Different designs of nozzle and diffuser in PZT-PEMFC (f = 8 Hz, t = 1 s).

inverter to invert the DC voltage into a higher AC voltage such as 50–150 V. For example, a typical inverter could invert DC 4.5 V to AC 110 V, which requires about 150 mW. Thus, in this case, a stack with a power higher than 150 mW is suitable for the PZT pack.

5. Conclusion

An innovative design for a PZT-PEMFC with a nozzle and diffuser (PZT-PEMFC-ND) which may solve the water-flooding problem with a high performance, was successfully built. The major experimental findings are as follows:

1. The pump performance of the PZT-PEMFC-ND is a function of the aspect ratio (AR) and diffuser angle (θ). The optimal geometry parameters AR is 11.25 under $\theta = 22.89^{\circ}$.
2. PZT vibration frequency and cell temperature are the major operating parameters for increasing the performance of the PZT-PEMFC-ND. The optimal PZT vibration frequency is $f = 180$ Hz under a temperature of 323 K.
3. Air intake, water removal rate, and cell performance are affected by the gravity effect and the orientation of the PZT's maximum vibration deflection. Both the L-PZT-R and L-PZT-D cases are the better designs in this study.
4. The power density can reach up to 0.18 W cm^{-2}, which is under $f = 180$ Hz and 0.6 V, approximately four times greater than the case without PZT vibration.
5. The PZT-PEMFC-ND, which needs 50–150 V and a low current a 0.1–0.01 A, is suitable to be installed as a stack or as a part of stack for removing the water.

Acknowledgement

This research was funded by the National Science Council of the Republic of China (NSC 96-2221-E-002-074-MY2)

References

[1] H.K. Ma, S.H. Huang, The 4th International Conference on Fuel Cell Science Engineering and Technology, 2006.
[2] X. Li, I. Sabir, Int. J. Hydrogen Energy 30 (2004) 359–371.
[3] W.M. Yan, C.H. Yang, C.Y. Soong, F. Chen, S.C. Mei, J. Power Sources 160 (2006) 284–292.
[4] X.D. Wang, Y.Y. Duan, W.M. Yan, X.F. Peng, J. Power Sources 175 (2007) 397–407.
[5] C. Xu, T.S. Zhao, Electrochem. Commun. 9 (2007) 497–503.
[6] Y. Wang, M. Ouyang, J. Power Sources 164 (2007) (2007) 721–729.
[7] D.T. Santa Rosa, D.G. Pinto, V.S. Silva, R.A. Silva, C.M. Rangel, Int. J. Hydrogen Energy 32 (2007) 4350–4357.
[8] L. Matamoros, D. Bruggemann, J. Power Sources 173 (2007) 367–374.
[9] S.U. Jeong, E.A. Cho, H.J. Kim, T.K. Lim, I.H. Oh, S.H. Kim, J. Power Sources 159 (2006) 1089–1094.
[10] S.U. Jeong, E.A. Cho, H.J. Kim, T.K. Lim, I.H. Oh, S.H. Kim, J. Power Sources 158 (2006) 348–353.
[11] P.L. Li, T. Zhang, Q.M. Wang, L. Schaefer, M.K. Chyu, J. Power Sources 2003 (2003) 63–69.
[12] T.F. Fuller, J. Newman, J. Electrochem. 139 (1992) 1332–1337.
[13] T.A. Zawodzinski, J. Davey, J. Valerio, S. Gottesfeld, Electrochim. Acta 40 (1995) 297–302.
[14] S.H. Ge, B.L. Yi, P.W. Ming, J. Electrochem. 153 (2006) A1443–A1450.
[15] M. Ise, K.D. Kreuer, J. Maier, Solid State Ionics 125 (1999) 213–223.
[16] T.E. Springer, T.A. Zawodzinski, S. Gottesfeld, J. Electrochem. Soc. 138 (1991) 2334–2342.
[17] J.S. Yi, T.V. Nguyen, J. Electrochem. Soc. 145 (1998) 1149–1159.
[18] S.H. Ge, B.L. Yi, J. Power Sources 124 (2003) 1–11.
[19] H. Li, Y. Tang, Z. Wang, Z. Shi, S. Wu, D. Song, J. Zhang, K. Fatih, J. Zhang, H. Wang, Z. Liu, R. Abouatallah, A. Mazza, J. Power Source 178 (2008) 103–117.
[20] A. Olsson, P. Enoksson, G. Stemme, E. Stemme, International Conference on Solid-State Sensors and Actuators, 1995, pp. 291–294.
[21] H. Takao, K. Miyamura, H. Ebi, M. Ashiki, K. Sawada, M. Ishida, International Conference on Solid-State Sensors, Actuators and Microsystems, 2003, pp. 139–142.
[22] X. Ying, Z. Zhou, H. Cho, X. Luo, Sens. Actuat. A Phys. 130–131 (2006) 531–536.
[23] H.K. Ma, S.H. Huang, B.R. Chen, L.W. Cheng, J. Power Sources 180 (2008) 402–409.
[24] H.K. Ma, S.H. Huang, Y.Z. Kuo, J. Power Sources 185 (2008) 1154–1161.
[25] H.K. Ma, S.H. Huang, J. Fuel Cell Sci. Technol. 6 (2009) 034501.
[26] H.K. Ma, S.H. Huang, B.R. Hou, L.W. Cheng, ASME 5th International Fuel Cell Science Engineering and Technology Conference, New York, 2007.
[27] H.K. Ma, S.H. Huang, Y.C. Kuo, ASME 6th International Fuel Cell Science, Engineering and Technology Conference, Denver Colorado, 2008.
[28] E. Stemme, G. Stemme, Sens. Actuat. A Phys. 39 (1993) 159–167.
[29] A. Olsson, P. Enoksson, G. Stemme, E. Stemme, J. Micromectromech. Syst. 6 (2) (1997) 161–166.
[30] M. Ahmadian, A. Mehrabian, J. Phys. 34 (2006) 379–384.
[31] H.K. Ma, S.H. Huang, C.C. Yu, C.G. Hou, Y.T. Chang, A. Su, in: ASME 7th International Fuel Cell Science, Engineering and Technology Conference, Newport Beach, California (2009).
[32] H.K. Ma, J.S. Wang, S.H. Huang, Y.J. Huang, Y.Z. Kuo, in: ASME 7th International Fuel Cell Science, Engineering and Technology Conference, Newport Beach, California (2009).
[33] Y.Y. Tsui, S.L. Lu, Sens. Actuat. A Phys. 148 (2008) 138–148.
[34] A. Ullmann, Sens. Actuat. A Phys. 69 (1998) 97–105.
[35] L.S. Pan, T.Y. Ng, G.R. Liu, K.Y. Lam, T.Y. Jiang, Sens. Actuat. A Phys. 93 (2001) 173–181.
[36] F.M. White, Fluid Mechanics, McGraw-Hill, New York, 1986, pp. 334–336.
[37] G.K. Artyushkina, Tr. LPI 333 (1973) 104–106.
[38] L. Levin, F. Clermont, Le Fĕnie Civil 140 (10) (1970) 11–20.
[39] V. Singhal, S.V. Garimella, J.Y. Murthy, Sens. Actuat. A Phys. 113 (2004) 226–235.
[40] J.P. Hartnett, M. Kostic, Adv. Heat Transfer 19 (1989) 247–356.
[41] K.S. Yang, I.Y. Chen, B.Y. Shew, C.C. Wang, J. Micromech. Microeng. 14 (2003) 26–31.
[42] J.H. Jang, H.C. Chiu, W.M. Yan, W.L. Sun, J. Power Sources 180 (2008) 476–483.
[43] W.M. Yan, X.D. Wang, S.S. Mei, X.F. Peng, Y.F. Guo, A. Su, J. Power Sources 185 (2008) 1040–1048.